Supporting Information

Synergistic Role of Cl^- and Br^- Ions in Growth Control and Mechanistic Insights of High Aspect Ratio Silver Nanowires for Flexible Transparent Conductive Films

*Jia-Lei Xu [a], Rui-Dong Shi [a], Hai-ping Zhou [a], Guo-Tao Xiang [a], Zi-Dong Zhou [a], Yong-Da Hu [*b], and Jin-Ju Chen [*a]*

a. School of Materials and Energy, University of Electronic Science and Technology of China, Chengdu 610054, P. R. China. E-mail: jinjuchen@uestc.edu.cn

b. School of Integrated Circuit Science and Engineering, University of Electronic Science and Technology of China, Chengdu 610054, P. R. China

Density functional theory (DFT) calculations

Density functional theory calculations were performed in the plane wave and ultrasoft pseudopotential framework, as implemented in the CASTEP suite of codes[1]. Based on the Koelling-Harmon method, relativistic effects was considered. Density mixing was used for the electronic structure, and Broyden-Fletcher-Goldfarb-Shanno (BFGS) geometry optimization has improved the indicated symmetry of crystal structure.

The electron exchange and correlation were described with the generalized-gradient approximation (GGA) and the Perdew-Burke-Ernzerhof (PBE) function[2]. Convergence of electronic self-consistent field cycles was accelerated by the The implementation of the Residual Minimization Method with Direct Inversion in the Iterative Subspace (RMM-DIIS).To accommodate the van der Waals interactions, the DFT-D method developed by Grimme et al. was used for dispersion corrections[3].

Optimization of bulk Ag. The bulk Ag structure (JCPDS: 04-0783) was optimized using a plane wave basis set with a cutoff energy of 550 eV. 6×6×6 Monkhorst-Pack k-point grid was employed for Brillouin zone integration. The smearing value is 0.1, which is the width of the smearing in eV. Electronic self-consistency was achieved when the energy change was less than 1×10^{-6} eV. During geometry optimization, convergence criteria were set to an energy change of 1×10^{-5} eV, a maximum force of 0.03 eV $Å^{-1}$, and a maximum displacement of 0.001 Å. Table S1 details the structural changes of bulk Ag before and after optimization, and

all slab models were constructed based on this optimized bulk Ag structure. As shown in Figure S1, the deviation between the theoretical value of the silver lattice parameter and the laboratory value is only 3%, indicating that the calculation method is highly reliable.

Simulation modeling calculations.

All slab surface models were constructed with parameters detailed in Table S2. The plane wave basis set cutoff energy was set to 500 eV. 2×2×1 Monkhorst-Pack k-point grid was utilized for Brillouin zone integration of the slab surfaces. Convergence tests for energy cutoff and number of k points are shown in Table S3, and the corresponding results show the reliability of the convergence conditions[4]. The smearing value is 0.1, which is the width of the smearing in eV. Convergence of electronic self-consistent field cycles was achieved when the energy change was less than 2×10^{-6} eV. A 15 Å vacuum region was applied to separate the repeated slabs, with the bottom three atomic layers fixed and the remaining layers relaxed during geometry optimization. For geometry optimization and energetics of the slab surface models, convergence criteria included an energy change of 2×10^{-5} eV, a maximum force of 0.05 eV $Å^{-1}$, and a maximum displacement of 0.002 Å.

The adsorption behaviors of Cl^-/Br^- on different computational models were investigated by comparing their adsorption energies ($\Delta E_{Cl-/Br-*}$), calculated according to the following equation:

$$\Delta E_{Cl-/Br-*} = E_{(slab + Cl-/Br-)} - E_{Cl-/Br-} - E_{slab}$$

where $E_{(slab + Cl-/Br-)}$ is the energy of the slab with adsorbed Cl^-/Br^-, E_{slab} is the slab energy, and $E_{Cl-/Br-}$ is the energy of the Cl^-/Br^- ions.

Molecular dynamics (MD) simulation

MD simulations were conducted using the Forcite code[5], employing the Condensed Molecular Potential for Atomistic Simulation Studies Ⅲ (COMPASS Ⅲ) force-field variables[6]. Periodic boundary conditions were applied in all three dimensions. The multiphase catalytic interface model was constructed using slab models from DFT calculations as the Ag growth layer and incorporating $C_2H_6O_2$, Fe^{3+}, Cl^-, and Br^- molecules/ions for the solution layer, in which the total concentration of halogen atoms in each system remains constant. (parameters are detailed in Table S4). Geometry structure optimization was performed after the addition of molecules and ions. For simulation models, convergence criteria included an energy change of 1×10^{-4} kcal mol^{-1}, a maximum force of 0.005 kcal mol^{-1} $Å^{-1}$, and a maximum displacement of 5×10^{-5} Å. Long-range Coulomb and van der Waals interactions were treated by Ewald summation and atom-based summation, respectively. The system was pre-equilibrated using an NVT (The preparation process of silver nanowires is based on constant temperature and volume conditions.) ensemble for 1000 ps at 300 K by using a Berendsen thermostat. A time step of 2 fs was employed and trajectories were stored at every 2 ps. The PPPM method with a precision of 10^{-3} was used for handling the long-range electrostatic interactions of atoms, and the van der Waals interactions were cut off at 12.5 Å. Under the same conditions, subsequent atomic

simulations were performed for 2000 ps (Ag multiple twin model: 1200 ps) and the last 1000 ps (Multiple twin Ag model: 600 ps) trajectories were utilized for analysis. As shown in Figures S2-7 f and Figure S9g, during the selected research time in MD, the total energy of the system fluctuated slightly, and its relative deviation was less than 3.5%, indicating that the system has reached equilibrium. Furthermore, the surface adsorption behavior is affected by the diffusion rate of the molecules/ions[7], and then the diffusion coefficient of the molecules/ions in the solution layer is calculated. In Figures S2-7 g and Figure S9h, during the selected research time in MD, the diffusion coefficient of the solution molecules/ions in the system fluctuated slightly, indicating that the adsorption behavior of the Ag surface was not affected by the diffusion of the solution molecules/ions during this period. Then, these results indicate that the statistical results of the selected research period have excel reliability in MD.

Table S1. Crystal structural parameter of Ag.

	Ag	
	experimental values[a]	computed values
a (Å)	4.086	4.213
b (Å)	4.086	4.213
c (Å)	4.086	4.213
α (°)	90	90
β (°)	90	90
γ (°)	90	90

[a] JCPDS: 04-0783

Table S2. DFT calculation parameters for Ag (100) and Ag (111) models.

	Ag (100)	Ag (111)
a (Å)	15.011	14.444
b (Å)	14.444	14.444
c (Å)[a]	22.076	21.128
Number of atoms	144 (Ag)	122 (Ag)

[a] Direction c contains a 15 Å thick vacuum layer.

Table S3. Energy cutoff and k-point convergence test for Ag (100) and Ag (111).

	Cutoff energies[a]			K-point grids[b]		
	Value(eV)	Absolute energy(eV)	Energy difference (eV atom^{-1}) [c]	Value	Absolute energy(eV)	Energy difference (eV atom^{-1}) [c]
Ag (100)	450	-400612.12	- -	1×1×1	-400614.92	- -
	500	-400613.64	0.0106	2×2×1	-400613.64	0.0089
	550	-400614.00	0.0025	3×3×1	-400612.94	0.0041
Ag (111)	450	-480736.90	- -	1×1×1	-480740.06	- -
	500	-480738.24	0.0109	2×2×1	-480738.24	0.0149
	550	-480738.56	0.0026	3×3×1	-480738.03	0.0018

[a] 2×2×1 Monkhorst-Pack k-point grid was utilized.

[b] Cutoff energy was set to 500 eV.

[c] The absolute value of the difference between the absolute energy of the current step and the absolute energy of the previous test step.

Table S4. Parameters of the solid-liquid interface models of Ag (100)-Cl^-, Ag (100)-Br^-, Ag (100)-Cl^--Br^-, Ag (111)-Cl^-, Ag (111)-Br^-, Ag (111)-Cl^--Br^- and Ag-Br^--Cl^- multiple twin using MD simulation.

	a (Å)	b (Å)	c (Å)	Solidoid number of atoms	Liquidoid number of atoms
Ag(100)-Cl^-	40.444	40.444	103.992[a]	980 (Ag)	3030 (C: 600, H: 1800, O: 600, Fe: 10, Cl: 20)
Ag(100)-Br^-	40.444	40.444	103.992[a]	980 (Ag)	3030 (C: 600, H: 1800, O: 600, Fe: 10, Br: 20)
Ag(100)-Cl^--Br^-	40.444	40.444	103.992[a]	980 (Ag)	3030 (C: 600, H: 1800, O: 600, Fe: 10, Cl: 10, Br: 10)
Ag(111)-Cl^-	40.030	40.444	104.790[a]	1120 (Ag)	3030 (C: 600, H: 1800, O: 600, Fe: 10, Cl: 20)
Ag(111)-Br^-	40.030	40.444	104.790[a]	1120 (Ag)	3030 (C: 600, H: 1800, O: 600, Fe: 10, Br: 20)
Ag(111)-Cl^--Br^-	40.030	40.444	104.790[a]	1120 (Ag)	3030 (C: 600, H: 1800, O: 600, Fe: 10, Cl: 10, Br: 10)
Multiple twin Ag-Br^--Cl^-	60	60	60	181 (Ag)	21170 (C: 4192, H: 12576, O: 4192, Fe: 70, Cl: 70, Br: 70)

[a] Direction c contains a 70 Å thick vacuum layer.

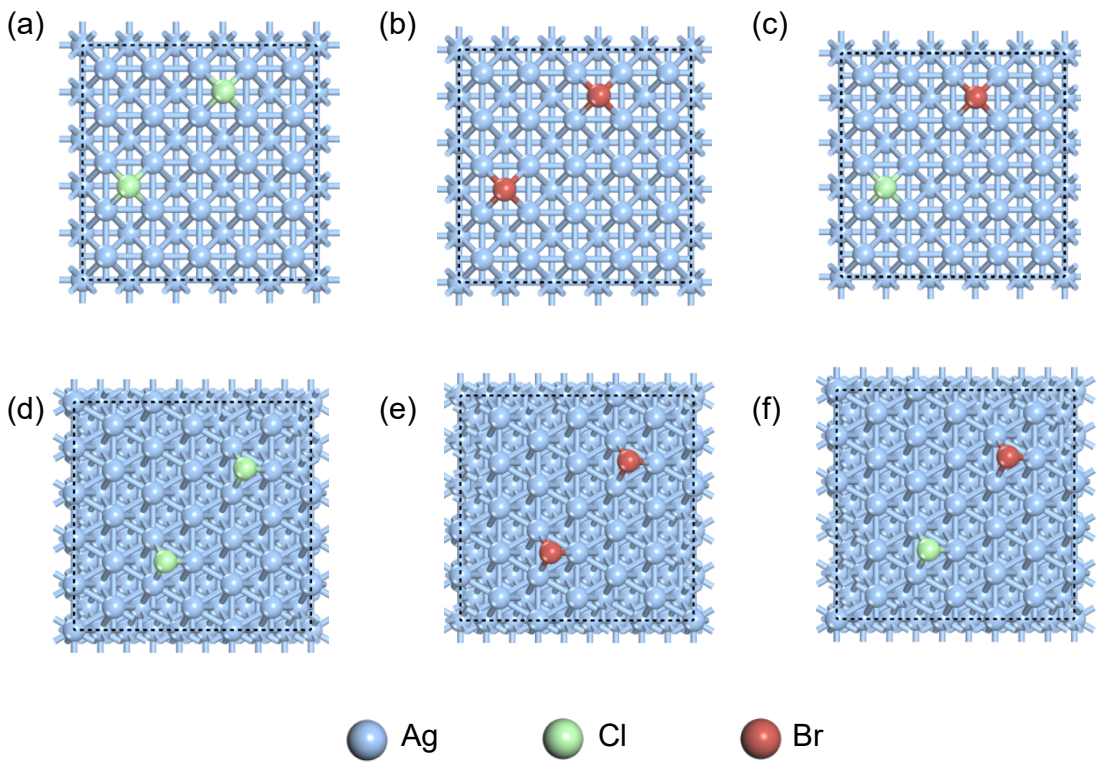

Figure S1. Top view of DFT calculation models of (a) Cl, (b) Br^-, and (c) Cl^--Br^- on Ag (100) surface. Top view of DFT calculation models of (d) Cl^-, (e) Br^-, and (f) Cl^--Br^- on Ag (111) surface.

Table S5 In DFT calculation, the coordinates of the halogen ions in the model after structural optimization.

Model	Halogen atomic coordinates[a] (Å)	
Ag(100)-Br^--Br^-	Br^-1 (2.829, 5.752, 8.584)	Br^-2 (8.725, 11.602,8.574)
Ag(100)-Cl^--Br^-	Cl (2.829, 5.744, 8.424)	Br (8.714, 11.597, 8.576)
Ag(100)-Cl^--Cl^-	Cl^-1 (2.828, 5.745, 8.418)	Cl^-2 (8.725, 11.604, 8.419)
Ag(111)-Br^--Br^-	Br^-1 (5.626, 2.141, 7.892)	Br^-2 (10.647, 8.021, 7.898)
Ag(111)-Cl^--Br^-	Cl^- (5.614, 2.137, 7.747)	Br^- (10.642, 8.013, 7.891)
Ag(111)-Cl^--Cl^-	Cl^-1 (5.597, 2.118, 7.743)	Cl^-2 (10.640, 8.019, 7.750)

[a] Cartesian coordinates

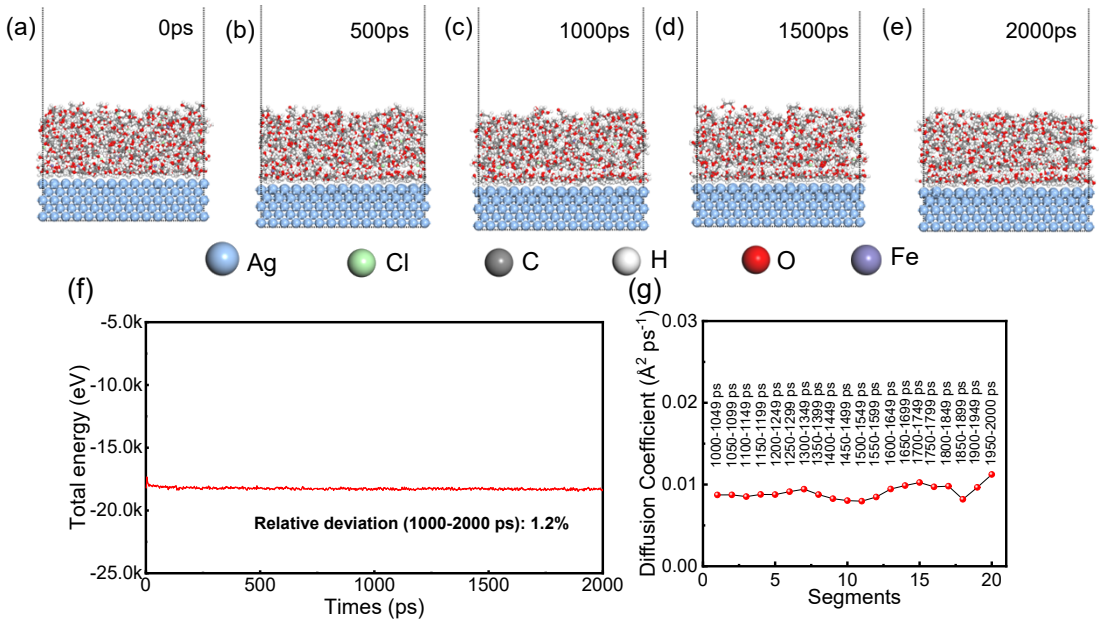

Figure S2. MD simulation snapshots of Cl^- adsorption on Ag (100) surface: (a) 0 ps, (b) 500 ps, (c) 1000 ps, (d) 1500 ps, and (e) 2000 ps. (f) Total energy evolution curve. (g) Diffusion coefficients between 1000 and 2000 ps (The sampling range is 50 ps).

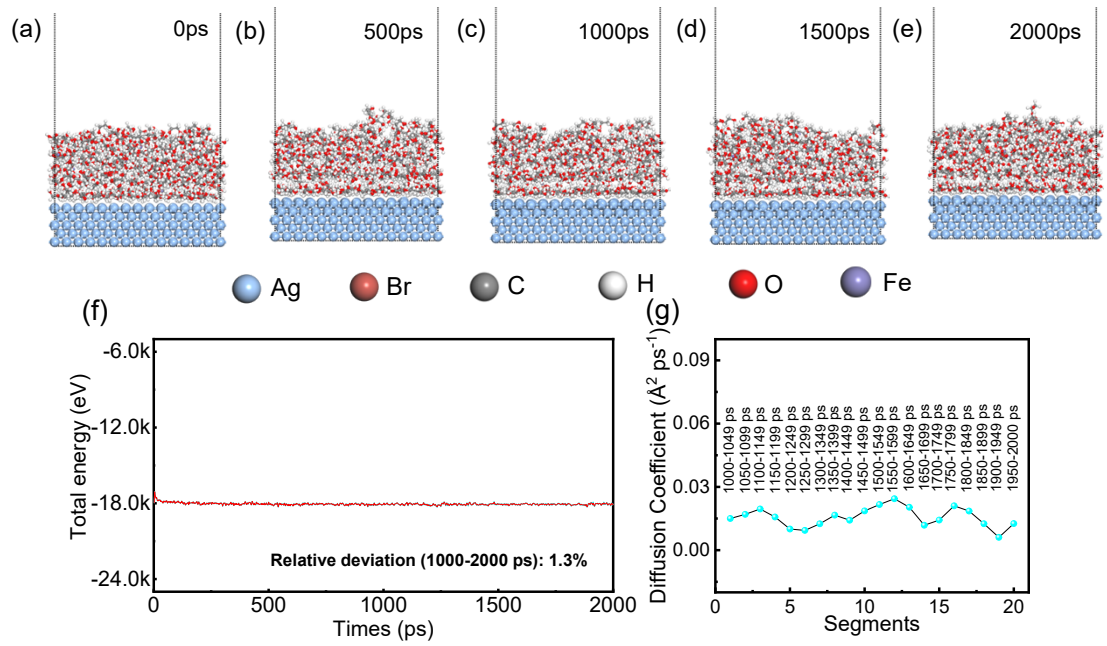

Figure S3. MD simulation snapshots of Br^- adsorption on Ag (100) surface: (a) 0 ps, (b) 50 0ps, (c) 1000 ps, (d) 1500 ps, (e) 2000 ps. (f) Total energy evolution curve. (g) Diffusion coefficients between 1000 and 2000 ps (The sampling range is 50 ps).

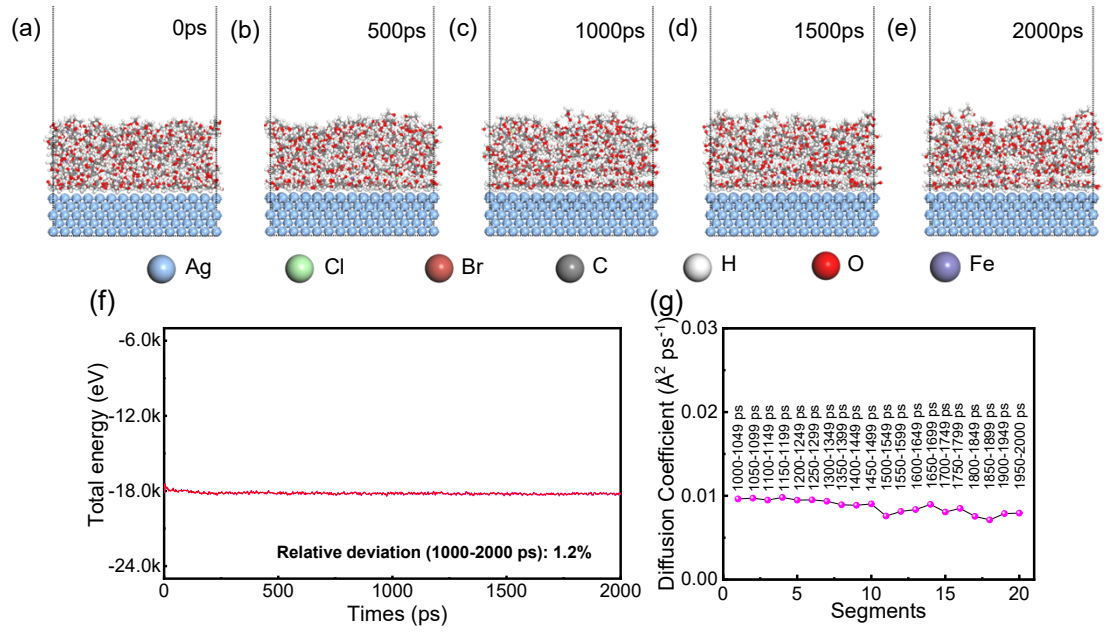

Figure S4. MD simulation snapshots of the adsorption of hybrid Cl^- and Br^- ions on Ag (100) surface: (a) 0 ps, (b) 500 ps, (c) 1000 ps, (d) 1500 ps, (e) 2000 ps. (f) Total energy evolution curve. (g) Diffusion coefficients between 1000 and 2000 ps (The sampling range is 50 ps).

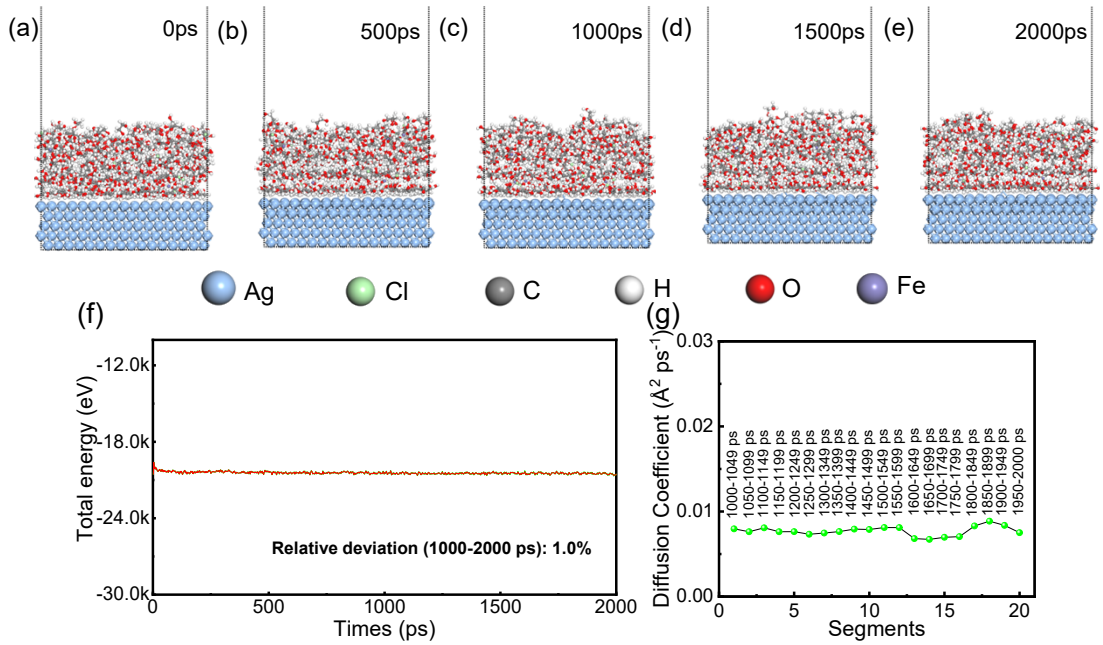

Figure S5. MD simulation snapshots of Cl^- adsorption on Ag (111) surface: (a) 0 ps, (b) 500 ps, (c) 1000 ps, (d) 1500 ps, (e) 2000 ps. (f) Total energy evolution curve. (g) Diffusion coefficients between 1000 and 2000 ps (The sampling range is 50 ps).

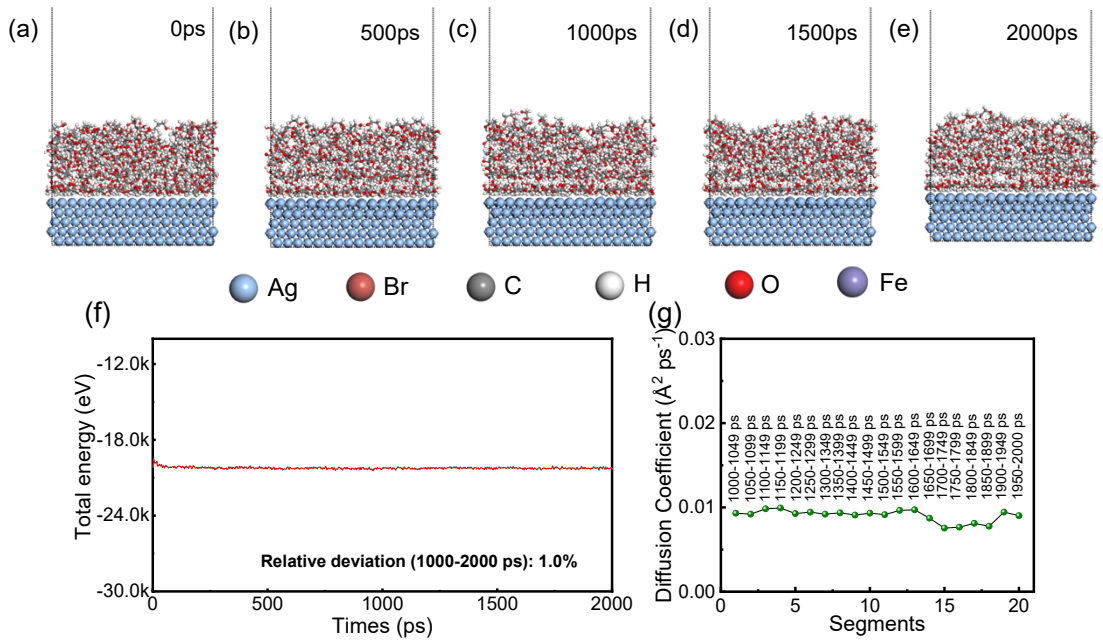

Figure S6. MD simulation snapshots of Br adsorption on Ag (111) surface, (a) 0 ps, (b) 500 ps, (c) 1000 ps, (d) 1500 ps, (e) 2000 ps. (f) Total energy evolution curve. (g) Diffusion coefficients between 1000 and 2000 ps (The sampling range is 50 ps).

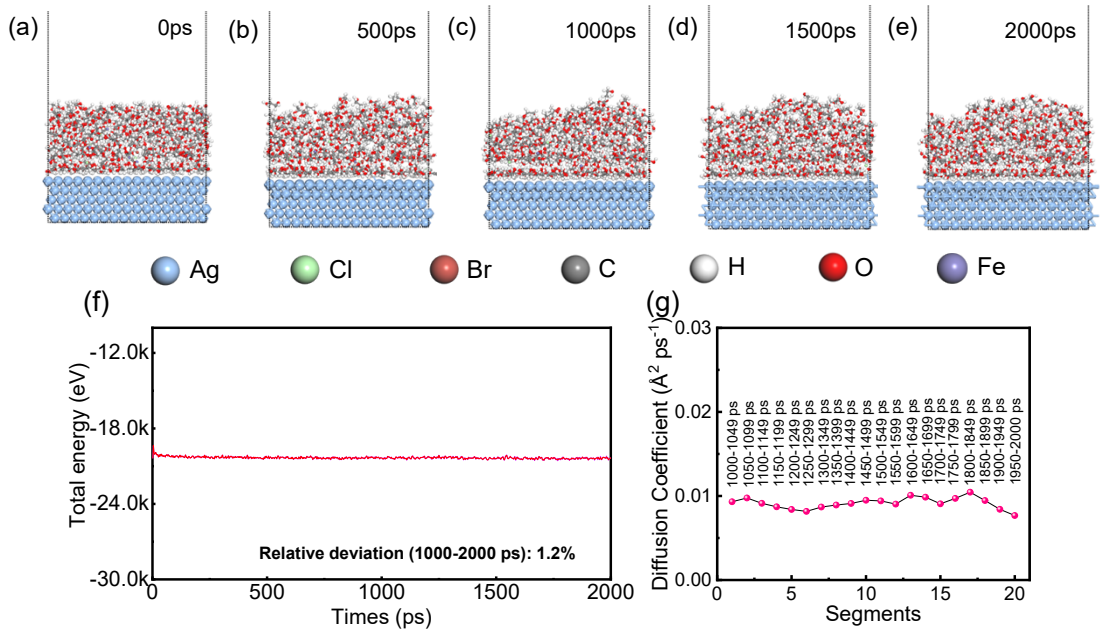

Figure S7. MD simulation snapshots of the adsorption of hybrid Cl^- and Br^- ions on Ag (111) surface, (a) 0 ps, (b) 500 ps, (c) 1000 ps, (d) 1500 ps, (e) 2000 ps. (f) Total energy evolution curve. (g) Diffusion coefficients between 1000 and 2000 ps (The sampling range is 50 ps).

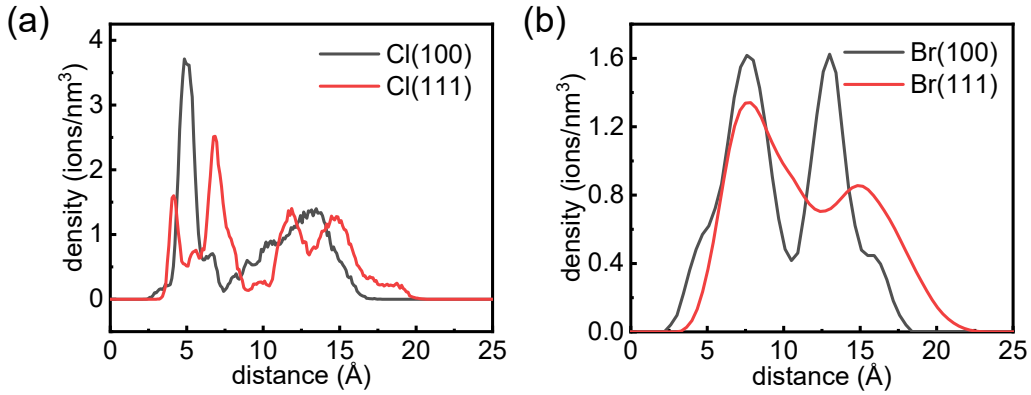

Figure S8. Ion density profiles of (a) Cl^- and (b) Br^- on Ag (100) and (111) surfaces as a function of the distance from the surface.

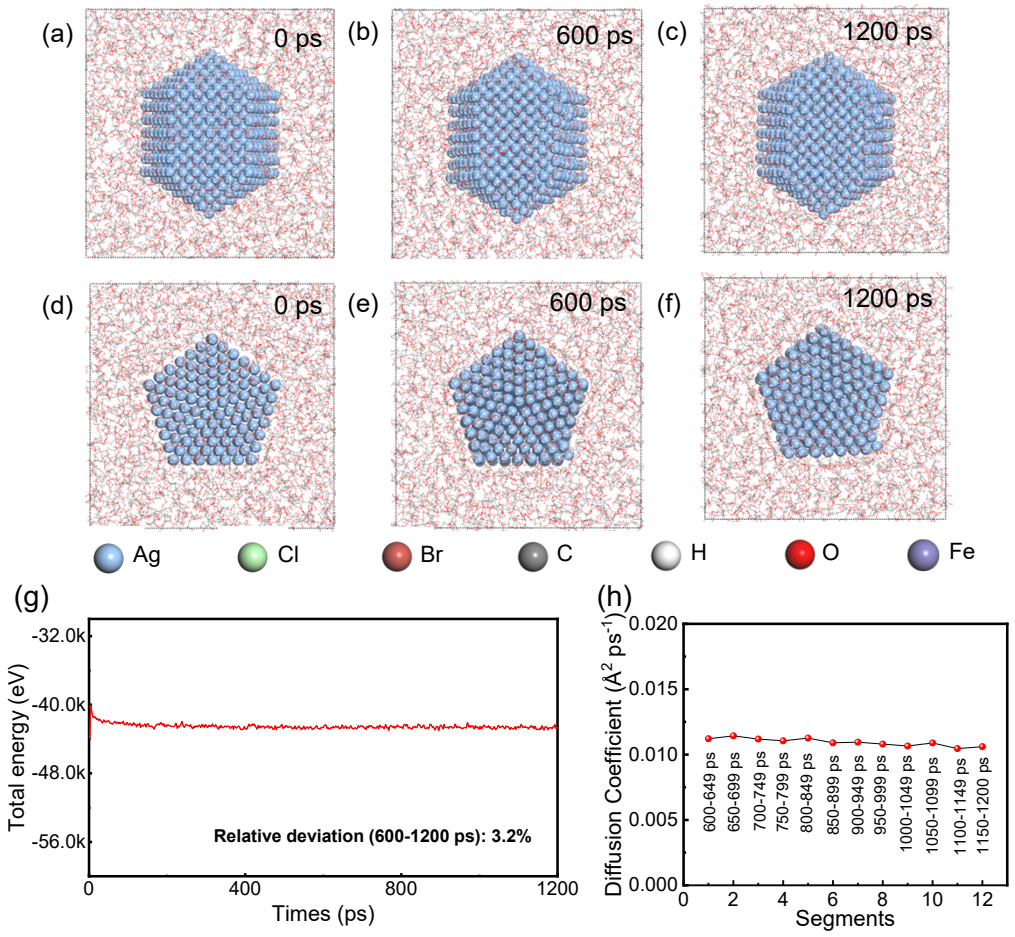

Figure S9. Snapshot of halogen ions adsorption on side of multiple twin nanoseed, (a) 0 ps, (b) 600 ps, and (c) 1200 ps. Snapshot of halogen ions adsorption on top of multiple twin nanoseed, (d) 0 ps, (e) 600 ps, and (f) 1200 ps. (g) Total energy evolution curve. (h) Diffusion coefficients between 600 and 1200 ps (The sampling range is 50 ps).

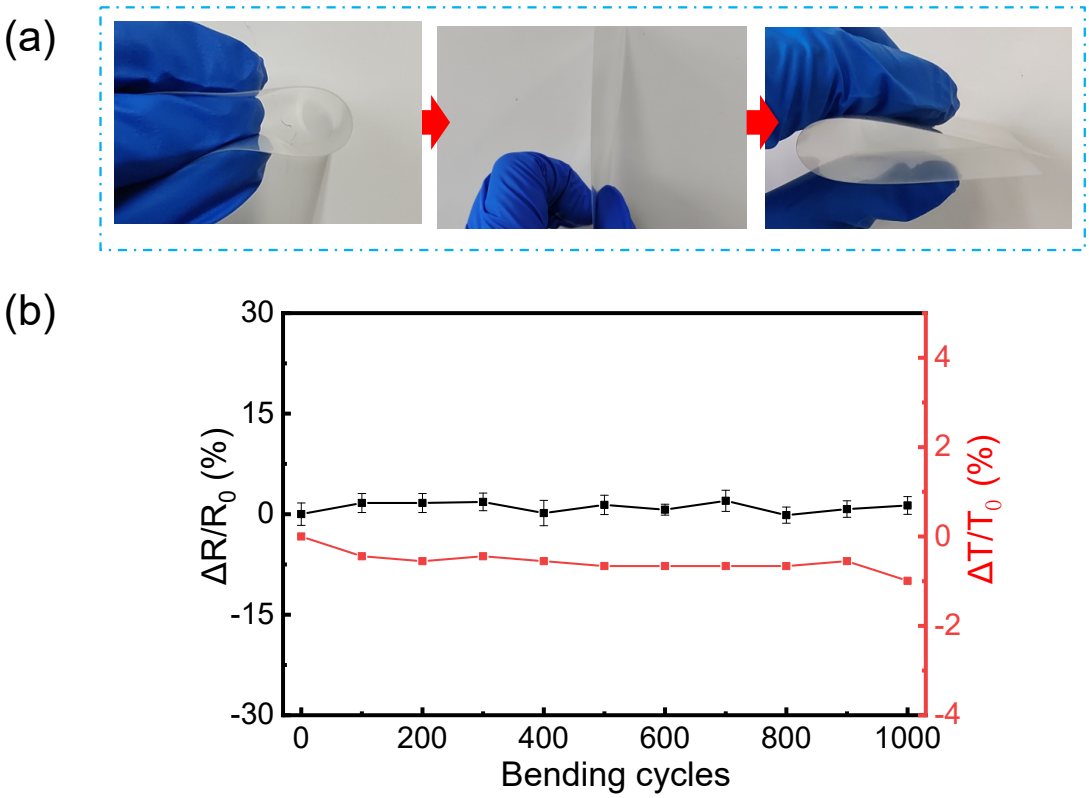

Figure S10 (a) The bending state of the TCF during one cycle (with a 6 mm bending radius), and (b) the variations in sheet resistance and light transmittance of the TCF across bending cycles.

Table S6**.** Comparative analysis of the latest studies on critical performance metrics of AgNWs and TCFs.

Length (μm)	Diameter (nm)	Aspect ratio	Transmittance (%)	Sheet resistance (Ω sq^{-1})	Reference
45	80	500	92.8	83.2	Ref. 8
35.7	67	500	83.9	22.3	Ref. 9
158	77	2000	84.7	12.6	Ref. 10
317	78	4000	98.2	61	Ref. 11
80	40	2000	86.7	68	Ref. 12
/	35	1500	95	20	Ref. 13
96	40	2400	95	14.7	this work

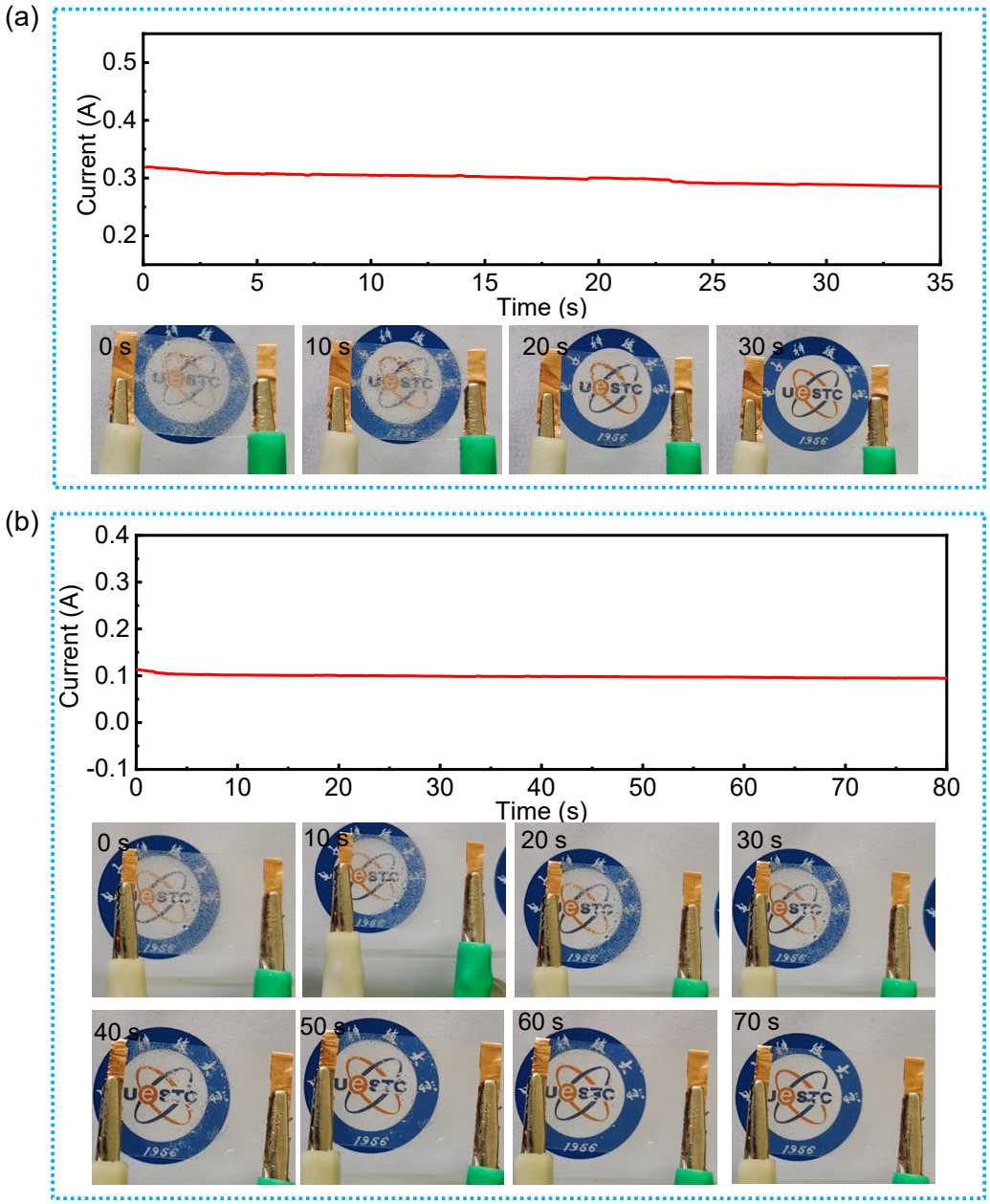

Figure S11 Defogging efficiency of TCFs with sheet resistances of (a) 24.2 Ω sq^{-1} and 46.5 Ω sq^{-1}.

References

1. S. J. Clark, M. D. Segall, C. J. Pickard, P. J. Hasnip, M. I. J. Probert, K. Refson and M. C. Payne, 2005, **220**, 567-570.
2. J. P. Perdew, K. Burke and M. Ernzerhof, *Physical Review Letters*, 1996, **77**, 3865-3868.
3. S. Grimme, *Journal of Computational Chemistry*, 2006, **27**, 1787-1799.
4. D. Yan, H. H. Kristoffersen, J. K. Pedersen and J. Rossmeisl, *ACS Catalysis*, 2022, **12**, 116-125.
5. G. J. Ackland, *Physical Review Letters*, 1998, **80**, 2233-2236.
6. H. Sun, Z. Jin, C. Yang, R. L. C. Akkermans, S. H. Robertson, N. A. Spenley, S. Miller and S. M. Todd, *Journal of Molecular Modeling*, 2016, **22**, 47.
7. F. Sun, H. Wang, Z. Qu, K. Wang, L. Wang, J. Gao, J. Gao, S. Liu and Y. Lu, *Advanced Energy Materials*, 2021, **11**, 2002981.
8. M. M. Rosli, T. H. T. A. Aziz, M. I. A. Umar, M. Nurdin and A. A. Umar, *Journal of Electronic Materials*, 2022, **51**, 5150-5158.
9. J. Zhou, Y. Zang, Y. Wang, L. Chu, G. Li, R. Xu and W. Yan, *Journal of Materials Science: Materials in Electronics*, 2023, **34**, 467.
10. L. Zhang, F. Jiang, B. Wu, C. Lv and M. Wu, *Nanotechnology*, 2021, **32**, 105710.
11. M. Yao, L. Zhao, C. Fan, X. Han, Z. Wu, H. Sun, G. Wang and R. Xiao, *Chemical Communications*, 2024, **60**, 8884-8887.
12. H. Ao, J. Feng, P. Cao, T. Yang, T. Shang and B. Xing, *Journal of Materials Science: Materials in Electronics*, 2023, **34**, 2183.
13. X. Zhu, A. Guo, J. Xu and C. Kan, *CrystEngComm*, 2020, **22**, 8421-8429.